



Anomalous phonon relaxation in Au₃₃₃(SR)₇₉ nanoparticles with nascent plasmons

Tatsuya Higaki^{a,1}, Meng Zhou^{a,1}, Guiying He^b, Stephen D. House^{c,d}, Matthew Y. Sfeir^{b,2}, Judith C. Yang^{c,d,e}, and Rongchao Jin^{a,3}

^aDepartment of Chemistry, Carnegie Mellon University, Pittsburgh, PA 15213; ^bCenter for Functional Nanomaterials, Brookhaven National Laboratory, Upton, NY 11973; ^cDepartment of Chemical and Petroleum Engineering, University of Pittsburgh, Pittsburgh, PA 15261; ^dEnvironmental Transmission Electron Microscopy Catalysis Consortium, University of Pittsburgh, Pittsburgh, PA 15261; and ^eDepartment of Physics and Astronomy, University of Pittsburgh, Pittsburgh, PA 15260

Edited by Catherine J. Murphy, University of Illinois at Urbana–Champaign, Urbana, IL, and approved May 22, 2019 (received for review March 12, 2019)

Research on plasmons of gold nanoparticles has gained broad interest in nanoscience. However, ultrasmall sizes near the metal-to-nonmetal transition regime have not been explored until recently due to major synthetic difficulties. Herein, intriguing electron dynamics in this size regime is observed in atomically precise Au₃₃₃(SR)₇₉ nanoparticles. Femtosecond transient-absorption spectroscopy reveals an unprecedented relaxation process of 4–5 ps—a fast phonon–phonon relaxation process, together with electron–phonon coupling (~1 ps) and normal phonon–phonon coupling (>100 ps) processes. Three types of –R capped Au₃₃₃(SR)₇₉ all exhibit two plasmon-bleaching signals independent of the –R group as well as solvent, indicating plasmon splitting and quantum effect in the ultrasmall core of Au₃₃₃(SR)₇₉. This work is expected to stimulate future work on the transition-size regime of nanometals and discovery of behavior of nascent plasmons.

atomically precise | gold nanoparticles | surface plasmon resonance | ultrafast spectroscopy | phonon relaxation

Plasmonics in nanoscale is being intensively studied owing to rich fundamental science (1–3). Recent advances in studies of plasmons and hot carriers have further accelerated the advancement of their applications into nanotechnology (4–6). To explore new functionalities of such materials, it is of fundamental importance to study the nascent state of surface plasmon resonance (SPR) and excited-state dynamics. For example, SPR disappears when the size goes down below 2 nm due to quantum confinement effect and quantization of the conduction band (7). Unlike the conventional, plasmonic gold nanoparticles of face-centered cubic structure, the ultrasmall gold nanoparticles (so-called nanoclusters) with discrete energy levels exhibit unique geometrical (8–10) and electronic structures (11–13), and novel properties for applications in biomedicine (14, 15), optoelectronics (16, 17), and catalysis (18, 19).

To explore new nanocluster materials and their novel functionalities, it is of fundamental importance to understand at what size and how the transition from nonmetallic to metallic state occurs, as well as the excited-state dynamics. Recently, a breakthrough has been made regarding the long-standing question on the birth of SPR (20–23). According to spectroscopic analysis (20, 21), a sharp transition from nonmetallic to metallic state occurs between Au₂₄₆(SR)₈₀ and Au₂₇₉(SR)₈₄, with a mere 33 gold atom difference. This abrupt transition is unexpected from the 50 y of theoretical prediction of a smooth transition by Kubo et al. (24). Although the nascent SPR in Au₂₇₉ showed single SPR and power-dependent lifetime in transient absorption (TA) measurements similar to conventional plasmonic nanoparticles (25, 26), a very long lifetime for phonon–phonon coupling process (>300 ps) was observed with broad excited-state absorption (ESA) in the near-infrared (NIR) region up to 1,600-nm wavelength (20). Such unique features of nascent SPR suggested the need of further exploration near the transition size

regime for gaining fundamental insights into the plasmon origin, as well as a search for intriguing properties. Future work may also include the effect of shape, surface, and the type of metal (e.g., Ag) on the transition (27–31).

Because of major difficulties in the synthesis of atomically precise plasmonic nanoparticles, the ultrasmall size regime (near 2 nm) has been hampered significantly. Previous studies by femtosecond spectroscopy for plasmonic nanoparticles with narrow distributions demonstrated the evolution of electron dynamics in the size range of 5–100 nm (32, 33). Upon photoexcitation with a pump pulse, the conduction electrons of metal nanoparticles become thermalized on the timescale of 10–100 fs via electron–electron scattering. The relaxation of excited metal nanoparticles undergoes two processes to release the energy. First, the energy in electronic excited state rapidly induces phonons of the metal lattice in 1–10 ps via electron–phonon coupling, and then the thermal energy of the lattice phonon is dissipated into the environment in >100 ps via phonon–phonon coupling. These time constants increase with the increase in pump fluence. The fundamental coupling times for electron–phonon and phonon–phonon interactions decrease with size

Significance

Plasmons and evolution from the metallic to nonmetallic state in metal nanoparticles (NPs) are being actively pursued in nanoscience research. Previous research has not been able to probe the fundamental science of nascent plasmons due to major difficulties in the synthesis of atomically precise NPs in the 2- to 3-nm range. Herein, we report intriguing ultrafast electron dynamics in ultrasmall, atomically precise Au₃₃₃(SR)₇₉ NPs (2.5-nm diameter). Femtosecond transient-absorption spectroscopy revealed an unprecedented relaxation process of 4–5 ps—an instantaneous phonon–phonon relaxation evidenced by the similarity in spectroscopic profiles. The unique dynamics of Au₃₃₃(SR)₇₉, plus plasmon splitting, is expected to stimulate future work on the ultrasmall size regime of nanometals with nascent plasmons.

Author contributions: R.J. designed research; T.H., M.Z., G.H., S.D.H., and M.Y.S. performed research; T.H., M.Z., G.H., S.D.H., M.Y.S., J.C.Y., and R.J. analyzed data; and T.H., M.Z., S.D.H., and R.J. wrote the paper.

The authors declare no conflict of interest.

This article is a PNAS Direct Submission.

Published under the PNAS license.

¹T.H. and M.Z. contributed equally to this work.

²Present addresses: Photonics Initiative, Advanced Science Research Center, City University of New York, New York, NY 10031; and Department of Physics, Graduate Center, City University of New York, New York, NY 10016.

³To whom correspondence may be addressed. Email: rongchao@andrew.cmu.edu.

This article contains supporting information online at www.pnas.org/lookup/suppl/doi:10.1073/pnas.1904337116/-DCSupplemental.

Published online June 17, 2019.

shrinking, as more efficient energy dissipation occurs with higher surface-to-volume ratios in smaller sizes (25, 26, 34, 35).

On the other hand, metal nanoclusters in nonmetallic (excitonic) state show multiple ground state-bleaching (GSB) bands (like organic molecules) upon photoexcitation (11–13, 36). The photogenerated exciton experiences a relaxation process of electron-hole recombination, and its lifetime depends on the size and structure. The lifetime of nanoclusters is independent of pump fluence, in contrast to that of plasmonic nanoparticles. However, accurate and systematic analyses for smaller plasmonic sizes near the plasmonic origin (e.g., between 2 and 4 nm) are still challenging, so the detailed spectroscopic studies are very limited (37–41). Therefore, fundamental research on metal particles in the ultrasmall size regime remains to be explored, especially the new optoelectronic behavior in such materials, as these will impact both scientific understanding of metallic-bond formation and practical applications in photocatalysis and solar energy conversion.

Here, we report the unique excited-state dynamics of Au₃₃₃(SR)₇₉ nanoclusters with nascent SPR. The Au₃₃₃(SR)₇₉ nanoclusters (with SR = 2-phenylethanethiolate, PET for short; 1-butanethiolate, SC₄; 1-hexanethiolate, SC₆) all show a single peak in the steady-state absorption spectrum at room temperature. Interestingly, cryogenic spectroscopic analysis shows peak splitting. Further studies by femtosecond TA spectroscopy reveal that Au₃₃₃ nanoclusters exhibit two distinct GSB signals. Global-fitting analyses of TA spectra demonstrate that the electron dynamics of Au₃₃₃ involves a 4- to 5-ps rapid phonon relaxation process in addition to the typical electron–phonon coupling (~1 ps) and thermal dissipation (>100 ps). This unprecedented process is regardless of the type of –SR thiolate. The fundamental coupling time of this unique phonon process in Au₃₃₃(PET)₇₉ is determined to be 3.9 ± 0.1 ps by power-dependence analysis. The two GSB bands and additional relaxation process are also independent of solvent polarity, suggesting that they originate from the unique geometry of metal core. These results may stimulate future studies on the ultrasmall sizes near the metal-to-nonmetal transition regime, and the fundamental insights will lead to enhanced or tailored functionality of metal nanoclusters with nascent plasmons.

Results and Discussion

Synthesis and Steady-State Absorption. The three types of Au₃₃₃(SR)₇₉ nanoclusters were synthesized via a size-focusing method developed by us in a previous report (42), but with some modifications (see *Experimental Procedures* for details). The steady-state optical absorption spectra of the three Au₃₃₃(SR)₈₄ nanoclusters with different –R groups (i.e., C₂H₄Ph,

C₄ and C₆) all showed a single peak at the same position (498 nm) at room temperature (Fig. 1A), with the spectra resembling that of conventional plasmonic nanoparticles of spherical shape (25, 26). The absorption spectrum of Au₃₃₃(PET)₇₉ was further measured at low temperatures, and interestingly, a new peak appeared at 442 nm with temperature decrease to 80 K (Fig. 1B), but the 498-nm peak remains unshifted from 300 K down to 80 K. The emergence of a new peak in Au₃₃₃(SR)₇₉ is intriguing and unprecedented, which differs from the typical behavior of plasmonic nanoparticles.

Ultrafast Electron Dynamics. To further probe the optical properties of Au₃₃₃(SR)₇₉, we chose Au₃₃₃(PET)₇₉ to perform a detailed analysis by femtosecond TA spectroscopy. Upon photoexcitation at 360 nm, the TA data maps of the Au₃₃₃(PET)₇₉ nanoclusters showed two GSB bands at 485 and 540 nm, together with broad ESA below 400-nm and above 600-nm regions (Fig. 2A and B). The dual GSB bands in the TA are distinctly different from that of typical plasmonic gold nanoparticles of spherical shape; the latter shows a single GSB at the same position as the steady-state absorption peak.

To further study the process and the dynamics, global fitting was performed for the TA data of Au₃₃₃(PET)₇₉ (Fig. 2C). The relaxation dynamics of excited nanoclusters consist of three processes with different lifetimes. The faster process ($\tau_{e-ph} = \sim 1$ ps) and slower process ($\tau_{ph-ph} = >100$ ps) were assigned to electron–phonon coupling and phonon–phonon coupling, respectively. The spectroscopic features in the faster and slower processes, i.e., strong net GSB with two ESA wings and weak featureless profiles, respectively, agree with the previously reported electron–phonon and phonon–phonon coupling processes for gold nanoparticles (25, 26). However, the Au₃₃₃(PET)₇₉ nanoclusters showed an unexpected third process with 5 ps in the relaxation dynamics. The two GSB bands in the spectral profile are consistent with the steady-state absorption peaks at cryogenic temperatures (Fig. 1B), including peak shifts of >20 nm reported for nascent SPR (20).

Laser power-dependence analysis was performed for Au₃₃₃(PET)₇₉ to clarify the origin of the observed unique relaxation process of 4–5 ps. Upon photoexcitation at 360 nm in toluene, fundamental coupling times from global fitting analyses were extracted as a function of pump fluence (Fig. 2D). Both decay processes (~1 and 4–5 ps) showed weak but certainly power-dependent dynamics, indicating that both processes originate from continuous-band electronic structure in metallic state (Fig. 2D and *SI Appendix*, Fig. S1). The extracted fundamental coupling times for ~1- and 4- to 5-ps processes were 3.9 ± 0.1 and 1.33 ± 0.05 ps, respectively. The kinetic traces probed at 485 and 565 nm (for ~1- and 4- to 5-ps processes, respectively) indeed showed different decays (*SI Appendix*, Fig. S2). According to the previous reports on the ligand-protected particles with amplified laser systems, the 1.33-ps relaxation is reasonable as the electron–phonon coupling process of Au₃₃₃ (25, 26, 40). Of note, the coupling time is even shorter under very low power measurements for colloidal gold nanoclusters or bare gold nanocluster embedded on Al₂O₃ (35). In contrast, the process of 4–5 ps has a quite long lifetime as an electron–phonon coupling, indicating the possibility for another relaxation process. Indeed, the spectral profile of the 4- to 5-ps process is blue-shifted compared with ~1-ps process, suggesting different thermalization processes following the e–ph interactions. Careful comparison of the normalized spectral profile with the three processes actually demonstrates that the 4- to 5-ps process shares a similar profile with the >100-ps process rather than the ~1-ps process (*SI Appendix*, Fig. S3). Considering its bleaching signal in the profile, the 4- to 5-ps process is thus assigned as the relaxation process of phonons, which is surprisingly faster than the case of typical plasmonic nanoparticles (typically >100 ps). It is worth noting that our assignment is consistent with previous literature

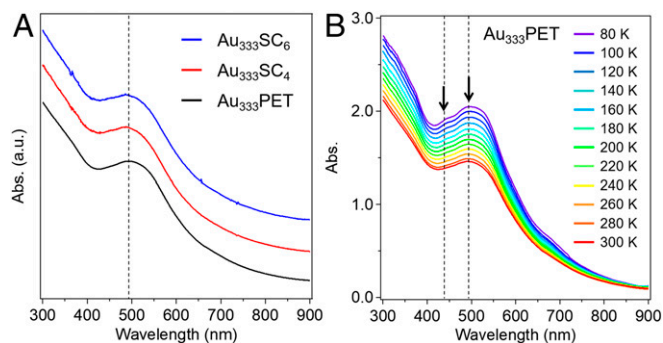


Fig. 1. Steady-state optical absorption spectra of Au₃₃₃(SR)₇₉. (A) Room temperature optical absorption of Au₃₃₃(PET)₇₉, Au₃₃₃(SC₄)₇₉, and Au₃₃₃(SC₆)₇₉ in dichloromethane. (B) Temperature-dependent steady-state optical absorption spectra of Au₃₃₃(PET)₇₉ in 2-methyl THF.

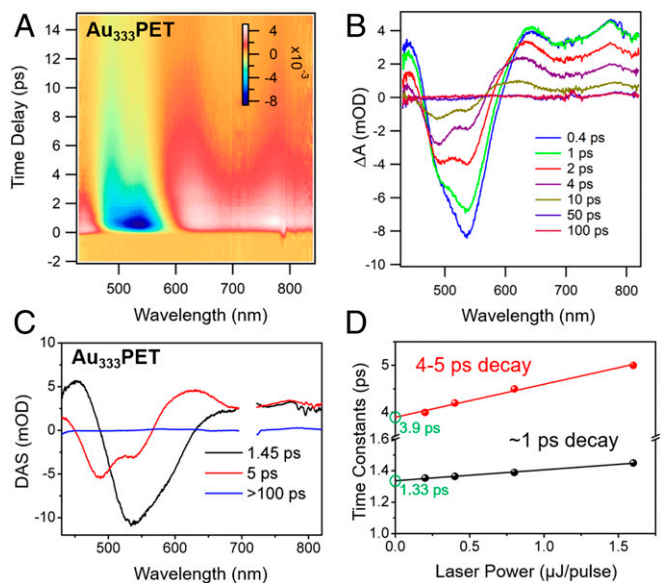


Fig. 2. TA spectra of Au₃₃₃(PET)₇₉ in toluene. (A) TA data map with pump pulse energy of 1.6 μJ/pulse. (B) TA spectra as a function of time delay between 0.4 and 100 ps. (C) Global-fitting analysis. (D) Extracted fundamental coupling times from global-fitting analyses for ~1-ps (black) and 4- to 5-ps (red) decays as a function of 360-nm excitation pump fluence for Au₃₃₃(PET)₇₉.

on metal nanoparticles about the core phonon relaxation shortening with decreasing size (34, 43). In our current work, the observation of two phonon–phonon relaxation processes (the anomalous 4- to 5-ps process plus the typical >100-ps one) is indeed unprecedented.

Of note, the linear TA intensity to the pump power rules out the possibility of multiphoton process for the 4- to 5-ps relaxation or impurities resulted from photodamage to the Au₃₃₃(PET)₇₉ nanocluster (SI Appendix, Fig. S4). Furthermore, TA with different excitation wavelengths was performed with 600 and 750 nm (in toluene), and the 4- to 5-ps process showed up independently (SI Appendix, Fig. S5), ruling out the plausible assignment of ~1- and 4- to 5-ps processes to intraband (*sp*) and interband (*d* to *sp*) relaxations, respectively.

The other two nanoclusters, Au₃₃₃(SC₄)₇₉ and Au₃₃₃(SC₆)₇₉, were also analyzed by TA spectroscopy (Fig. 3 A and B). Upon photoexcitation at 360 nm, both Au₃₃₃(SR)₇₉ nanoclusters also showed GSB bands at 485 and 540 nm, indicating that the unique features in TA are common for Au₃₃₃(SR)₇₉ with different types of thiolates. Therefore, the observed GSB bands do not depend on the carbon tail structure. Global-fitting analyses on Au₃₃₃(SC₄)₇₉ and Au₃₃₃(SC₆)₇₉ also exhibited three processes: the faster process ($\tau_{e-ph} \sim 1$ ps), the slower process ($\tau_{ph-ph} > 100$ ps), and the unusual process [5.6 and 4.5 ps for Au₃₃₃(SC₄)₇₉ and Au₃₃₃(SC₆)₇₉, respectively] (Fig. 3 C and D).

The potential solvent dependence was examined for Au₃₃₃(PET)₇₉ to obtain deeper insights into the relaxation process. The TA measurements for Au₃₃₃(PET)₇₉ in tetrahydrofuran (THF) and benzene were performed and are summarized in Fig. 4 for comparison with the dynamics in toluene. The instantaneous phonon relaxation is commonly observed in all of the solvents, also with similar peak positions according to global-fitting analyses (SI Appendix, Table S1). Thermal dissipation of excited gold nanoparticles is reported to depend on the heat capacity of the solvent based on the different efficiency in heat transfer. Therefore, the unique phonon relaxation process in the Au₃₃₃ occurs inside the core, followed by thermal dissipation to the environment in >100 ps.

Overall, the similar peak positions summarized in SI Appendix, Table S1 demonstrate that the two unique features (i.e., the 4- to 5-ps phonon–phonon coupling process and splitting of GSB into two bands) should originate from the geometrical feature of the metal core, with no significant influence from the thiolate’s –R group or solvent polarity as demonstrated above.

High-Angle Annular Dark-Field Scanning Transmission Electron Microscopy Analysis. To investigate the structural origin of the unique 4- to 5-ps process, Au₃₃₃(PET)₇₉ is studied by high-angle annular dark-field scanning transmission electron microscopy (HAADF-STEM) analysis. Aberration-corrected STEM analysis of the nanoparticles confirmed a high degree of uniformity in size and shape (SI Appendix, Fig. S6 A and B). The nanoparticles have a mean diameter of 2.17 nm and SD of 0.06 nm (SI Appendix, Fig. S6C), in excellent agreement with the expected size by the number of atoms. Higher-magnification observations of the nanoparticles confirmed their crystallinity (SI Appendix, Fig. S7 A–C). The measured atomic lattice spacings were consistent with the face-centered cubic structure revealed by power X-ray diffraction. Image intensity profiles were acquired from many nanoparticles and shown in SI Appendix, Fig. S7 D–F; the oscillations are from the periodic nature of the atomic planes/columns. The profiles of the nanoparticles were predominantly plateau-like, indicating a broader and flatter top facet compared with the rounder, vicinal perimeter surfaces (SI Appendix, Fig. S7 D–F). A more spherical or hemispherical nanoparticle would exhibit a more convex, arched intensity profile. The measured plane spacings and slightly oblong hexagonal arrangement of the atomic columns visible in the particles indicates that the flat top facets are [110] type (SI Appendix, Fig. S7 G and H). Of note, even at the low beam currents used, the surface atoms of the nanoparticles exhibited some degree of mobility, which would help explain the variations in perimeter shape observed—while retaining consistent overall size and top facet orientation.

Conclusion

In this work, the observed plasmon splitting and electron dynamics of Au₃₃₃(SR)₇₉ are intriguing and remarkable. Steady-state absorption spectra revealed two absorption peaks at 442 and 498 nm at 80 K, which is different from the case of typical

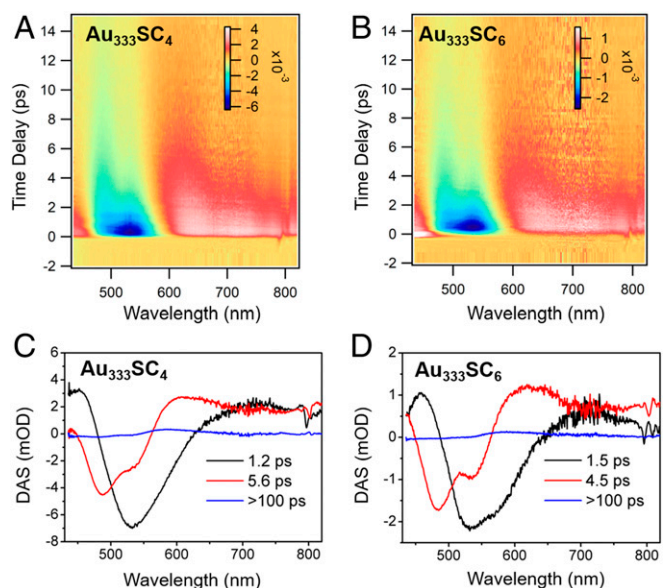


Fig. 3. TA data map (Top) and global-fitting analysis (Bottom); Au₃₃₃(SC₄)₇₉ (A and C), and Au₃₃₃(SC₆)₇₉ (B and D) pumped at 360 nm in toluene.

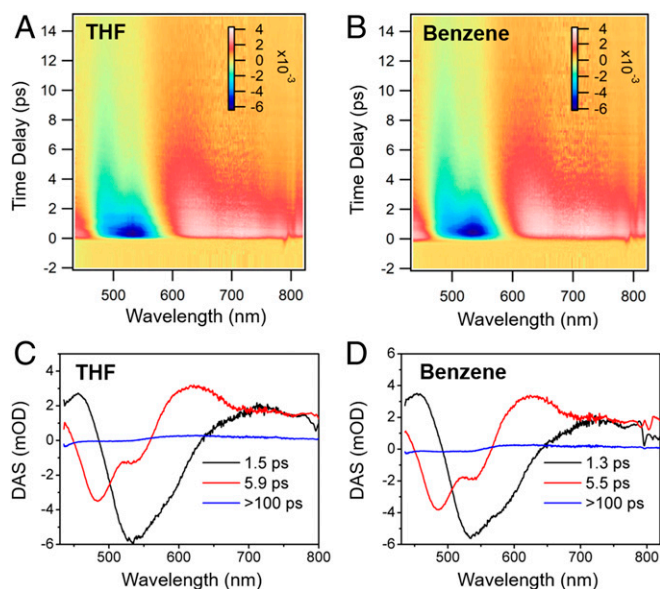


Fig. 4. Solvent-independent dynamics of $\text{Au}_{333}(\text{PET})_{79}$. TA data map (A and B) and global-fitting analysis for electron dynamics of $\text{Au}_{333}(\text{PET})_{79}$ in THF (A and C) and benzene (B and D).

plasmonic nanoparticles. The laser fluence dependence of both peaks indicates that both are plasmon peaks (as opposed to excitons) (11–13, 40). The dual plasmons indicate a nonspherical shape of Au_{333} . Of note, its atomic structure has not been determined yet. The splitting of SPR band in $\text{Au}_{333}(\text{SR})_{79}$ could be ascribed to an oblate core, which would give rise to splitting of plasmon. The statement is partially supported by HAADF-STEM analysis of the Au_{333} nanoparticles. Previous work on oblate nanostructures (e.g., nanoprisms) indeed showed an unusual plasmon below that of spherical particle's plasmon wavelength, e.g., a 320-nm out-of-plane quadrupole plasmon of Ag nanoprisms versus the ~ 390 -nm dipolar plasmon for spherical Ag nanoparticles (4). Multiple plasmons in the ultrasmall size regime were also reported to be related to the d band screening effect (44). Future work on the determination of the total structure of $\text{Au}_{333}(\text{SR})_{79}$ will eventually reveal the origin of its plasmon splitting.

The TA spectra of $\text{Au}_{333}(\text{SR})_{79}$ with different $-R$ groups revealed that the two GSB signals are not dependent on the ligand's carbon tail, nor the solvents (e.g., toluene, THF, and benzene). Global-fitting analyses revealed that the unusual process has a decay lifetime of 4–5 ps, whereas the ~ 1 -ps electron–phonon coupling and the >100 -ps phonon–phonon coupling times are typical of plasmonic gold nanoparticles. The test of laser power dependence at 485 nm confirmed that the 4- to 5-ps relaxation process showed power-dependent dynamics, with the extracted coupling time being 3.9 ps, which is larger than the 1.33 ps for the electron–phonon coupling time. The kinetic traces at the two peak positions (485 and 565 nm) indeed show different decay dynamics, where the peak at 565-nm decays to zero in ~ 4 ps, but the peak at 485 nm takes more than ~ 10 ps, indicating a difference in the origin of the two relaxation processes (*SI Appendix, Fig. S2*); in other words, the additional 4- to 5-ps process is not due to e–p coupling, whereas the 1-ps process is. We believe that the unique flat shape of Au_{333} should be a key to the intriguing 4- to 5-ps ph–ph process, albeit it remains to be confirmed by theoretical simulation (which is very demanding for such a large-sized cluster) (45).

The discoveries of an unusual relaxation process and plasmon splitting in $\text{Au}_{333}(\text{SR})_{79}$ nanoclusters with nascent SPRs may

stimulate further studies on the ultrasmall size regime of metal nanoparticles in the future, in particular theoretical analysis. The combined experiment and theory will lead to the discovery of other intriguing phenomena in this ultrasmall size regime and intriguing functionalities of this unusual type of materials.

Experimental Procedures

Chemicals. Chemicals were as follows: tetrachloroauric(III) acid ($\text{HAuCl}_4 \cdot 3\text{H}_2\text{O}$, $>99.99\%$ metals basis; Aldrich), tetrabutylammonium bromide (TOAB) ($\geq 98\%$; Fluka), 2-phenylethanethiol (PET) ($\text{C}_6\text{H}_5\text{SH}$, 98%; Aldrich), 1-butanethiol (SC_4 , $\text{C}_4\text{H}_9\text{SH}$; Acros Organics), 1-hexanethiol (SC_6 , $\text{C}_6\text{H}_{13}\text{SH}$; Acros Organics), and sodium borohydride (NaBH_4 ; Aldrich). Solvents were as follows: methanol (HPLC grade, $\geq 99.9\%$; Aldrich), dichloromethane (ACS reagent, $\geq 99.5\%$; Aldrich), toluene (HPLC grade, $\geq 99.9\%$; Aldrich), 2-methyltetrahydrofuran (anhydrous, inhibitor-free, $\geq 99\%$; Aldrich), THF (HPLC grade, $\geq 99.9\%$; Fisher Chemical), and benzene (HPLC grade, $\geq 99.9\%$; Aldrich). All chemicals were used without further purification. Nanopure water was prepared with a Barnstead NANOpure Diamond system.

Synthesis. The $\text{Au}_{333}(\text{SR})_{79}$ nanoclusters were synthesized by the size focusing and solvent fractionation, according to previously reported methods with slight modification (41, 42). For typical synthesis of $\text{Au}_{333}(\text{PET})_{79}$, 100 mg of $\text{HAuCl}_4 \cdot 3\text{H}_2\text{O}$ was dissolved in 5 mL of nanopure water and 160 mg of TOAB was dissolved in 10 mL of toluene. They were mixed in a 100-mL round-bottom flask. Then the solution was vigorously stirred for 15 min to allow all of the Au(III) salt in the aqueous phase to be transferred into the organic phase with the aid of TOA^+ . The colorless aqueous phase [no Au(III) salt left] was removed by a glass pipette. Then, 70 μL of PET was added to the flask using a syringe. The color of the toluene phase changed from dark red-orange to pale yellow and eventually colorless. The solution was kept stirring for 30 min. Subsequently, 96 mg of NaBH_4 (dissolved in 5 mL of ice cold nanopure water) was rapidly added to the reaction flask. The color of the reaction mixture immediately turned black, indicating the formation of gold nanoclusters. After 30 min, the aqueous phase was discarded by a glass pipette, and the organic phase was dried by rotary evaporation. The as-obtained polydisperse $\text{Au}_x(\text{PET})_y$ nanoparticles were washed with methanol three times to remove excess thiol and other side products.

The size-focusing methodology was applied to convert the initially polydisperse gold nanoclusters into specific-sized gold nanoclusters [containing $\text{Au}_{144}(\text{PET})_{60}$, $\text{Au}_{333}(\text{PET})_{79}$, and $\text{Au}_{\sim 519}(\text{PET})_{\sim 104}$] (42). Typically, ~ 50 mg of polydisperse $\text{Au}_x(\text{PET})_y$ nanoclusters obtained from step I were dissolved in 1 mL of toluene and 1 mL of PET. The solution was heated to 80°C and maintained at this temperature under air atmosphere with gentle stirring. After ~ 4 d of etching, $\text{Au}_{144}(\text{PET})_{60}$, $\text{Au}_{333}(\text{PET})_{79}$, and $\text{Au}_{\sim 519}(\text{PET})_{\sim 104}$ survived as stable gold nanocluster species (left in the solution). Then, the product nanoclusters were separated from the thiol/toluene solution by adding excess methanol and further centrifugation at 10,000 rpm for 3 min. The supernatant (which contains excess thiol) was discarded, and the black precipitate (containing the product nanoclusters) was washed with methanol three times. Then, the product nanoclusters were extracted from the precipitate by methylene chloride.

Finally, the solvent fractionation methodology was applied to isolate $\text{Au}_{333}(\text{PET})_{79}$ from the mixture of specific-sized gold nanoclusters [containing $\text{Au}_{144}(\text{PET})_{60}$, $\text{Au}_{333}(\text{PET})_{79}$, and $\text{Au}_{\sim 519}(\text{PET})_{\sim 104}$]. Typically, ~ 19 mg of crude product is dissolved in 1 mL of methylene chloride. The solution is transferred to 1.5-mL microcentrifuge tube with 0.5 mL of acetone. After centrifugation for 3 min, supernatant is discarded. This process is repeated with stepwise increase of methylene chloride portion (e.g., methylene chloride/acetone = 1.0/0.5, 1.1/0.4, 1.2/0.3, and so on) until complete removal of $\text{Au}_{144}(\text{PET})_{60}$ from the mixture. Then, $\text{Au}_{333}(\text{PET})_{79}$ was extracted with mixed solvent of toluene and methanol (2:1 in vol/vol). The typical yield of $\text{Au}_{333}(\text{PET})_{79}$ was ~ 1.9 mg ($\sim 3\%$ in gold atom basis).

$\text{Au}_{333}(\text{SC}_4)_{79}$ and $\text{Au}_{333}(\text{SC}_6)_{79}$ nanoclusters were synthesized by following the same procedure but replacing PET with SC_4 and SC_6 , respectively. For solvent fractionation, toluene/acetonitrile was used to isolate $\text{Au}_{333}(\text{SR})_{79}$ from the mixture of gold nanoclusters as reported previously (41).

Steady-State UV-Vis-NIR and Cryogenic Spectroscopy. UV-Vis-NIR spectra of Au nanoclusters were acquired on a UV-3600 Plus UV-VIS-NIR spectrophotometer (Shimadzu) at room temperature. The temperature-dependent experiments were carried out on a home-built system comprising the UV3600Plus spectrometer, an Optistat CF2 cryostat (Oxford Instruments), a temperature controller, and a vacuum pump. 2-Methyltetrahydrofuran was used as the

solvent in the temperature range between 80 and 300 K for a clear glass measurement.

Ultrafast Optical Measurements. Femtosecond TA spectroscopy was carried out using a commercial Ti:sapphire laser system (Spitfire; Spectra Physics). Briefly, the ~100-fs laser pulses in the UV and NIR regions of the spectrum were generated by a 3.5-mJ regenerative amplifier system (Spitfire; Spectra-Physics) and optical parametric amplifier (OPA) (TOPAS, Light Conversion). A small portion of the laser fundamental was focused into a sapphire plate to produce supercontinuum in the visible range, which overlapped in time and space with the pump. Multiwavelength transient spectra were recorded using dual spectrometers (signal and reference) equipped with array detectors whose data rates exceeded the repetition rate of the laser (1 kHz). Solutions of clusters in 1-mm pathlength cuvettes were excited by the tunable output of the OPA (pump). All of the measurements were performed in toluene, benzene, and THF, and the optical density of the solutions was adjusted to be about 0.3 OD at the excitation wavelength. During the measurement, Teflon-coated magnetic bar was used to stir the sample constantly and the UV-Vis spectrum remained the same before and after the femtosecond experiments.

Data Analysis on the Electron Dynamics. Chirp correction has been made before the global analysis. Before global fitting, singular value decomposition has been performed to evaluate the number of time constants needed. Subsequently, the TA map was global fitted with a parallel model to give decay-associated spectra (DAS); the change of concentration can be described as $c_i^{para}(t) = \exp(-t/\tau_i)$.

HAADF-STEM Analysis. Specimens for transmission electron microscopy (TEM) were prepared by suspending the Au₃₃₃(PET)₇₉ nanoparticles in dichloromethane and drop-casting 4 μL of the solution onto ultrathin carbon-coated Cu TEM grids (Ted Pella). The specimen was allowed to dry in air, and then pumped down overnight in a vacuum desiccator. The TEM examination was performed using a Thermo Scientific Titan Themis G2 aberration-corrected scanning TEM operated at 200 kV in HAADF mode. The probe current was

set to 15 pA, to reduce beam exposure, as a sensitivity of these nanoparticles to higher current densities was observed.

As seen in *SI Appendix, Fig. S6*, and in the full-range histogram in *SI Appendix, Fig. S9*, a small number of larger nanoparticles were observed (e.g., the small secondary peaks in the histogram, centered at 3 and 3.4 nm). Closer examination of these nanoparticles strongly suggests that most of them are merely multiple Au₃₃₃ nanoparticles that have coalesced at some point during sample preparation and observation. First, coalescence of particles in close proximity could be induced to rapidly coalesce with higher or longer exposure. Especially if a beam shower was performed on an area to limit carbon buildup, nearby particles in the area would coalesce. Au₃₃₃ nanoparticles that were not in near proximity to another appeared to be immune to this effect and maintained their original size, even with extended beam showers at high beam currents. Second, most of these larger nanoparticles were composed of multiple grains, with each grain being approximately the same size as an individual Au₃₃₃ particle. Partially merged particles, easily identified by their lobed or oblong morphology, were automatically excluded from the histogram measurement collection by placing limits upon the circularity of acceptable particles (0.8–1.0). To help mitigate coalescence, by minimizing beam exposure, the probe current was kept low (15 pA) and the nominal magnification was kept to below 2M \times .

ACKNOWLEDGMENTS. R.J. acknowledges financial support from the National Science Foundation (DMR-1808675) and the Air Force Office of Scientific Research. This research used resources of the Center for Functional Nanomaterials, which is a US Department of Energy Office of Science Facility, at Brookhaven National Laboratory under Contract DE-SC0012704. S.D.H. and J.C.Y. acknowledge the financial support of Department of Energy Basic Energy Sciences through Grant DE FG0203ER15476, National Science Foundation Designing Materials to Revolutionize and Engineer Our Future under Contract CHE-1534630, and the Environmental Transmission Electron Microscopy Catalysis Consortium (funded by the University of Pittsburgh and Hitachi High Technologies Corporation). The TEM work was performed at the Nanoscale Fabrication and Characterization Facility, a laboratory of the Gertrude E. and John M. Petersen Institute of NanoScience and Engineering, housed at the University of Pittsburgh.

- E. Ozbay, Plasmonics: Merging photonics and electronics at nanoscale dimensions. *Science* **311**, 189–193 (2006).
- H. A. Atwater, A. Polman, Plasmonics for improved photovoltaic devices. *Nat. Mater.* **9**, 205–213 (2010).
- M. R. Jones, N. C. Seeman, C. A. Mirkin, Programmable materials and the nature of the DNA bond. *Science* **347**, 1260901 (2015).
- R. Jin *et al.*, Controlling anisotropic nanoparticle growth through plasmon excitation. *Nature* **425**, 487–490 (2003).
- K. Wu, J. Chen, J. R. McBride, T. Lian, Efficient hot-electron transfer by a plasmon-induced interfacial charge-transfer transition. *Science* **349**, 632–635 (2015).
- L. Zhou *et al.*, Quantifying hot carrier and thermal contributions in plasmonic photocatalysis. *Science* **362**, 69–72 (2018).
- H. Qian, M. Zhu, Z. Wu, R. Jin, Quantum sized gold nanoclusters with atomic precision. *Acc. Chem. Res.* **45**, 1470–1479 (2012).
- R. Jin, C. Zeng, M. Zhou, Y. Chen, Atomically precise colloidal metal nanoclusters and nanoparticles: Fundamentals and opportunities. *Chem. Rev.* **116**, 10346–10413 (2016).
- S. Wang *et al.*, Total structure determination of surface doping [Ag₄₆Au₂₄(SR)₃₂](BPh₄)₂ nanocluster and its structure-related catalytic property. *Sci. Adv.* **1**, e1500441 (2015).
- S. Yamazoe *et al.*, Hierarchy of bond stiffnesses within icosahedral-based gold clusters protected by thiolates. *Nat. Commun.* **7**, 10414 (2016).
- T. Zhao, P. J. Herbert, H. Zheng, K. L. Knappenberger, Jr, State-resolved metal nanoparticle dynamics viewed through the combined lenses of ultrafast and magneto-optical spectroscopies. *Acc. Chem. Res.* **51**, 1433–1442 (2018).
- S. H. Yau, O. Varnavski, T. Goodson, III, An ultrafast look at Au nanoclusters. *Acc. Chem. Res.* **46**, 1506–1516 (2013).
- S. Mustalhti *et al.*, Photodynamics of a molecular water-soluble nanocluster identified as Au₁₃₀(pMBA)₅₀. *J. Phys. Chem. C* **119**, 20224–20229 (2015).
- A. D. Kurdekar *et al.*, Streptavidin-conjugated gold nanoclusters as ultrasensitive fluorescent sensors for early diagnosis of HIV infection. *Sci. Adv.* **4**, eaar6280 (2018).
- B. Du *et al.*, Glomerular barrier behaves as an atomically precise bandpass filter in a sub-nanometre regime. *Nat. Nanotechnol.* **12**, 1096–1102 (2017).
- M. A. Abbas, P. V. Kamat, J. H. Bang, Thiolated gold nanoclusters for light energy conversion. *ACS Energy Lett.* **3**, 840–854 (2018).
- H. Zhang *et al.*, Bacteria photosensitized by intracellular gold nanoclusters for solar fuel production. *Nat. Nanotechnol.* **13**, 900–905 (2018).
- H. Chen *et al.*, Visible light gold nanocluster photocatalyst: Selective aerobic oxidation of amines to imines. *ACS Catal.* **7**, 3632–3638 (2017).
- X.-K. Wan, J.-Q. Wang, Z.-A. Nan, Q.-M. Wang, Ligand effects in catalysis by atomically precise gold nanoclusters. *Sci. Adv.* **3**, e1701823 (2017).
- T. Higaki *et al.*, Sharp transition from nonmetallic Au₂₄₆ to metallic Au₂₇₉ with nascent surface plasmon resonance. *J. Am. Chem. Soc.* **140**, 5691–5695 (2018).
- M. Zhou *et al.*, On the non-metallicity of 2.2 nm Au₂₄₆ (SR)₈₀ nanoclusters. *Angew. Chem. Int. Ed.* **56**, 16257–16261 (2017).
- C. Zeng, Y. Chen, K. Kirschbaum, K. J. Lambright, R. Jin, Emergence of hierarchical structural complexities in nanoparticles and their assembly. *Science* **354**, 1580–1584 (2016).
- N. A. Sakthivel, S. Theivendran, V. Ganeshraj, A. G. Oliver, A. Dass, Crystal structure of faradaurate-279: Au₂₇₉(SPh-tBu)₈₄ plasmonic nanocrystal molecules. *J. Am. Chem. Soc.* **139**, 15450–15459 (2017).
- R. Kubo, A. Kawabata, S. Kobayashi, Electronic properties of small particles. *Annu. Rev. Mater. Sci.* **14**, 49–66 (1984).
- G. V. Hartland, Optical studies of dynamics in noble metal nanostructures. *Chem. Rev.* **111**, 3858–3887 (2011).
- S. Link, M. A. El-Sayed, Optical properties and ultrafast dynamics of metallic nanocrystals. *Annu. Rev. Phys. Chem.* **54**, 331–366 (2003).
- A. Kawabata, R. Kubo, Electronic properties of fine metallic particles. II. Plasma resonance absorption. *J. Phys. Soc. Jpn.* **21**, 1765–1772 (1966).
- I. Chakraborty *et al.*, Emergence of metallicity in silver clusters in the 150 atom regime: A study of differently sized silver clusters. *Nanoscale* **6**, 8024–8031 (2014).
- C. Yu *et al.*, Optical properties of size selected neutral Ag clusters: Electronic shell structures and the surface plasmon resonance. *Nanoscale* **10**, 20821–20827 (2018).
- Y. Song *et al.*, Large-scale synthesis, crystal structure, and optical properties of the Ag₁₄₆Br₂(SR)₈₀ nanocluster. *ACS Nano* **12**, 9318–9325 (2018).
- H. Yang *et al.*, Plasmonic twinned silver nanoparticles with molecular precision. *Nat. Commun.* **7**, 12809 (2016).
- C. Voisin, N. Del Fatti, D. Christofilos, F. Vallée, Ultrafast electron dynamics and optical nonlinearities in metal nanoparticles. *J. Phys. Chem. B* **105**, 2264–2280 (2001).
- E. Minutella, F. Schulz, H. Lange, Excitation-dependence of plasmon-induced hot electrons in gold nanoparticles. *J. Phys. Chem. Lett.* **8**, 4925–4929 (2017).
- M. Hu, G. V. Hartland, Heat dissipation for Au particles in aqueous solution: Relaxation time versus size. *J. Phys. Chem. B* **106**, 7029–7033 (2002).
- A. Arbouet *et al.*, Electron-phonon scattering in metal clusters. *Phys. Rev. Lett.* **90**, 177401 (2003).
- C. Zeng *et al.*, Structural patterns at all scales in a nonmetallic chiral Au₁₃₃(SR)₅₂ nanoparticle. *Sci. Adv.* **1**, e1500045 (2015).
- Y. Negishi *et al.*, A critical size for emergence of nonbulk electronic and geometric structures in dodecanethiolate-protected Au clusters. *J. Am. Chem. Soc.* **137**, 1206–1212 (2015).
- R. Philip, P. Chantharasupawong, H. Qian, R. Jin, J. Thomas, Evolution of nonlinear optical properties: From gold atomic clusters to plasmonic nanocrystals. *Nano Lett.* **12**, 4661–4667 (2012).
- O. Varnavski, G. Ramakrishna, J. Kim, D. Lee, T. Goodson, Critical size for the observation of quantum confinement in optically excited gold clusters. *J. Am. Chem. Soc.* **132**, 16–17 (2010).

40. M. Zhou *et al.*, Evolution from the plasmon to exciton state in ligand-protected atomically precise gold nanoparticles. *Nat. Commun.* **7**, 13240 (2016).
41. K. Kwak, V. D. Thanthirige, K. Pyo, D. Lee, G. Ramakrishna, Energy gap law for exciton dynamics in gold cluster molecules. *J. Phys. Chem. Lett.* **8**, 4898–4905 (2017).
42. H. Qian, Y. Zhu, R. Jin, Atomically precise gold nanocrystal molecules with surface plasmon resonance. *Proc. Natl. Acad. Sci. U.S.A.* **109**, 696–700 (2012).
43. A. Stella *et al.*, Size effects in the ultrafast electronic dynamics of metallic tin nanoparticles. *Phys. Rev. B Condens. Matter* **53**, 15497–15500 (1996).
44. A. Manjavacas, F. J. García de Abajo, Tunable plasmons in atomically thin gold nanodisks. *Nat. Commun.* **5**, 3548 (2014).
45. P. Maioli *et al.*, Mechanical vibrations of atomically defined metal clusters: From nano- to molecular-size oscillators. *Nano Lett.* **18**, 6842–6849 (2018).